



Hypersonic and dielectric studies of disordered single crystals,  $\text{Rb}_{1-x}(\text{ND}_4)_x\text{D}_2\text{AsO}_4$ ,  $\text{Na}_{1/2}\text{Bi}_{1/2}\text{TiO}_3$  and  $\text{PbMg}_{1/3}\text{Nb}_{2/3}\text{O}_3$ , by Brillouin scattering and dielectric measurements  
by Chi-Shun Tu

A thesis submitted in partial fulfillment of the requirements for the degree of Doctor of Philosophy in  
Physics  
Montana State University  
© Copyright by Chi-Shun Tu (1994)

Abstract:

Temperature and frequency dependent measurements of dielectric permittivity, acoustic sound velocity and damping have been carried out by using Brillouin light scattering and a capacitance and conductance component analyzer on two different types of ferroelectrics, i.e. (i) FE-AFE mixed deuterium glasses  $\text{Rb}_{1-x}(\text{ND}_4)_x\text{D}_2\text{AsO}_4$  ( $x=0, 0.10, 0.28$ ), (ii) relaxor ferroelectrics  $\text{Na}_{1/2}\text{Bi}_{1/2}\text{TiO}_3$  (NBT) and  $\text{PbMg}_{1/3}\text{Nb}_{2/3}\text{O}_3$  (PMN).

In this study, three important results have been observed: (1) A broad and high-value maximum in dielectric permittivity has been observed in relaxors NBT and PMN, which indicates that these materials could be used for electrostrictive displacement transducers. (2) In FE-AFE mixed glasses DRADA- $x$ , a  $\eta_2\mu$ -type quadratic coupling, squared in order parameter and linear in strain, becomes the main coupling contribution as ammonium  $\text{ND}_4$  concentration  $x$  increases from 0 to an intermediate value. The results also confirm the presence of PE/FE phase coexistence in DRADA-0.10. (3) For both FE-AFE mixed glasses and relaxor ferroelectrics, the order parameter(s) fluctuations, which are generated by the local random fields originating from short-range randomly-placed cations, are the main dynamic mechanisms for hypersonic and dielectric anomalies. In DRADA-0.10 and 0.28, these local randomly-placed ions are  $\text{ND}_4^+$  and  $\text{Rb}^+$  ions. In PMN, those randomly-placed cations are  $\text{Mg}^{+2}$  and  $\text{Nb}^{+5}$  which are randomly placed at B-site positions. In NBT, those randomly-placed cations are  $\text{Na}^{+1}$  and  $\text{Bi}^{+3}$  which are placed randomly at A-site positions.

Two models, i.e. superparaelectric cluster and extrinsic bulk conductivity, also have been proposed to explain the high-temperature and low-frequency dielectric anomaly in NBT. The elastic stiffness and compliance constants are also calculated for PMN.

HYPERSONIC AND DIELECTRIC STUDIES OF DISORDERED SINGLE  
CRYSTALS,  $\text{Rb}_{1-x}(\text{ND}_4)_x\text{D}_2\text{AsO}_4$ ,  $\text{Na}_{1/2}\text{Bi}_{1/2}\text{TiO}_3$  AND  $\text{PbMg}_{1/3}\text{Nb}_{2/3}\text{O}_3$ , BY  
BRILLOUIN SCATTERING AND DIELECTRIC MEASUREMENTS

by

Chi-Shun Tu

A thesis submitted in partial fulfillment  
of the requirements for the degree

of

Doctor of Philosophy.

in

Physics

MONTANA STATE UNIVERSITY  
Bozeman, Montana

September, 1994

D378

T79

APPROVAL

of a thesis submitted by

Chi-Shun Tu

This thesis has been read by each member of the thesis committee and has been found to be satisfactory regarding content, English usage, format, citations, bibliographic style, and consistency, and is ready for submission to the college of Graduate Studies.

Oct. 3, 1994  
Date

V. Hugo Schmidt  
Chairperson, Graduate Committee

Approved for the Major Department

10-3-94  
Date

W. W. W. W.  
Head, Major Department

Approved for the College of Graduate Studies

10/30/94  
Date

P. A. Brown  
Graduate Dean

## STATEMENT OF PERMISSION TO USE

In presenting this thesis in partial fulfillment of the requirements for a doctoral degree at Montana State University, I agree that the Library shall make it available to borrowers under rules of the Library. I further agree that copying of this thesis is allowable only for scholarly purpose, consistent with "fair use as prescribed in the U.S. Copyright Law". Requests for extensive copying or reproduction of this thesis should be referred to University Microfilms International, 300 North Zeeb Road, Ann Arbor, Michigan 48106, to whom I have granted "the exclusive right to reproduce and distribute my dissertation for sale in and from microform or electronic format, along with the right to reproduce and distribute my abstract in any format in whole or in part."

Signature



Date

Oct. 3, 1994

*to my wife Rong-Mei (Ruth), because of whom all things are possible,  
and to my son Stachus, in whom I find the reasons*

## VITA

The author was born Chi-Shun Tu on January 21, 1962 in Kaohsiung, Taiwan. He is the fourth child of Rou-Nu Tu (deceased) and Hsiu-Hsia Tsai Tu and has three older sisters and one younger brother. He was married to Rong-Mei (Ruth) Chien in 1988 and has one son, Stachus Igu Tu.

The author finished his undergraduate work with a B.S in physics at National Taiwan Normal University in 1985. After that time, he was in the Army for two full years to complete his obligation and then taught physics at high school for another two years. From Sept. of 1988 to June of 1990, he attended the University of Oregon in Eugene, Oregon, and graduated with a M.S. in physics. In September of 1990, he enrolled at Montana State University as a graduate teaching and research assistant until the fall of 1994, obtaining a Ph.D. in physics under Professor V. Hugo Schmidt.

## ACKNOWLEDGMENTS

I would like to sincerely thank my advisor Prof. V. Hugo Schmidt for his support, advice, and encouragement over the past four years. Whenever I became confused or frustrated by the experiments, he was there with the appropriate advice and help. Dr. Igor G. Siny and Greg Pastalan helped me to set up the experimental system and taught me Brillouin scattering skills. I give Igor and Greg my appreciation for sharing their ideas with me and for so much technical guidance that was given freely.

Thanks to Prof. G.F. Tuthill for endless theoretical teaching and discussion, to Bob Parker for his technical support on computer software and hardware issues, to Dr. Toby Howell who helped me to learn dielectric measurements, and to Norm Williams and Erik Anderson for their technical help and friendship.

My wife Rong-Mei (Ruth) deserves my deepest appreciation for her constant support, encouragement and sacrifices. Stachus my son I rely upon to always bring a smile to my face and my heart.

My appreciation also goes to the National Science Foundation for the support I received under grant number DMR-9017429.

Finally, I would like to thank my parents, especially my mother. She gave us much help during the first six months since Stachus was born and during writing the thesis. They may not understand what I am doing, but they understand me. Their encouragement and support played an important role in the completion of this thesis.

## TABLE OF CONTENTS

	Page
1 INTRODUCTION.....	1
Introduction to Disordered Crystals.....	1
Relaxor Ferroelectrics (RF).....	3
Proton (or Deuteron) Glasses (PG).....	7
Previous Knowledge for Crystals Discussed in This Work.....	11
$\text{Na}_{1/2}\text{Bi}_{1/2}\text{TiO}_3$ (NBT).....	11
$\text{PbMg}_{1/3}\text{Nb}_{2/3}\text{O}_3$ (PMN).....	11
$\text{Rb}_{1-x}(\text{ND}_4)_x\text{D}_2\text{AsO}_4$ (DRADA- $x=0, 0.10$ and $0.28$ ).....	13
Purpose and Outline of The Present Work.....	13
2. EXPERIMENTAL PROCEDURES.....	15
Crystal Growth and Sample Preparation.....	15
Dielectric Permittivity.....	16
Brillouin Light Scattering.....	17
General Description of Experiment.....	18
Characteristics of the Fabry-Perot Interferometer.....	25
Pre-Alignment of Fabry-Perot Interferometer.....	29
Brillouin Spectrum Analysis.....	30
3. THEORY.....	34
Dielectric.....	34
Dipolar Relaxation Equations.....	38
Superparaelectric Model (Nano-Scale Polar Cluster).....	40
Equivalent Circuits of Dielectric Function.....	44
Brillouin Light Scattering.....	44
Spectrum and Principle of Brillouin Scattering.....	44
The Relation Between Velocity and Elastic Stiffness.....	54
Selection Rules of Scattered Light.....	65
Static Coupling Theory of First-Order Phase Transition.....	71
Debye Anharmonic Approximation.....	74
Dynamic Effects.....	75

TABLE OF CONTENTS—CONTINUED

	Page
4. RESULTS AND DISCUSSION.....	76
Rb <sub>1-x</sub> (ND <sub>4</sub> ) <sub>x</sub> D <sub>2</sub> AsO <sub>4</sub> (x=0, 0.10 and 0.28).....	76
Brillouin Back-Scattering Along LA[100] Phonon Direction.....	76
Na <sub>1/2</sub> Bi <sub>1/2</sub> TiO <sub>3</sub> (NBT).....	87
Frequency Dependent Dielectric Results.....	87
Superparaelectric Cluster Model.....	88
Surface-Modified Bulk Effect.....	94
Extrinsic Bulk Conductivity Model.....	95
Brillouin Backscattering Along LA[001] Phonon Direction.....	108
PbMg <sub>1/3</sub> Nb <sub>2/3</sub> O <sub>3</sub> (PMN).....	116
Dielectric and Brillouin Scattering Results.....	116
Determination of Elastic Stiffness Constants.....	123
5. CONCLUSIONS.....	126
Comparison of Results.....	126
Similarities Among PMN, NBT and DRADA-0.10 and 0.28.....	126
Differences Among PMN, NBT and DRADA-0.10 and 0.28.....	127
Applications.....	128
Recommended Additional Work on This Problem.....	130
REFERENCES CITED.....	132

## LIST OF TABLES

Table	Page
1. Parameters from the fits of Eq. (113) to measured values of frequency shift at high temperature.....	77
2. The parameters from fits of Eq. (34) to the real part of permittivity ( $\epsilon'$ ) at five temperatures.....	93
3. Elastic stiffness and compliance constants of PMN at several temperatures from two scattering geometries $\theta_s = 180^\circ$ and $32.5 \pm 0.2^\circ$ .....	125
4. Comparison of elastic stiffness and compliance constants at room temperature.....	125

## LIST OF FIGURES

Figure	Page
1. Two-dimensional illustration of ordered and disordered states for both FE-AFE mixed glasses $A_x(\text{NH}_4)_{1-x}\text{H}_2\text{BO}_4$ [or $A_x(\text{ND}_4)_{1-x}\text{D}_2\text{BO}_4$ ] and complex relaxor ferroelectric systems $(A_1A_2)\text{BO}_3$ , $A(\text{B}_1\text{B}_2)\text{O}_3$ .....	2
2. A perovskite cubic unit cell. The point group usually is $m\bar{3}m$ for a paraelectric cubic $\text{ABO}_3$ perovskite-type structure. Solid lines indicate the $\text{BO}_6$ octahedron. $A_4$ indicates one of three 4-fold rotation axes and $4mm$ is the usual corresponding point group in the tetragonal ferroelectric phase. $A_3$ indicates one of four 3-fold rotation axes and $3m$ is the usual corresponding point group in the trigonal ferroelectric phase.....	4
3. Mixed-ion arrangements of (a) ordered and (b) disordered cubic perovskite $\text{ABO}_3$ structure.....	6
4. A general schematic phase diagram vs. temperature for complex relaxor ferroelectrics. "?" indicates one or two intermediate regions.....	7
5. The structure of KDP at room temperature. Here just a few hydrogen bonds are shown.....	7
6. Projection of KDP along c-axis in the ferroelectric phase ( $T < T_c$ ). The solid line inside the square connects oxygen atoms at the same height.....	8
7. The structure of ADP projected along the c-axis. A $\text{NH}_4^+$ at height 0 is shown attached to nearby oxygens of $\text{PO}_4$ tetrahedra. The heights in unit of $c$ of the phosphorus centers of the $\text{PO}_4$ tetrahedral are indicated. The $\text{PO}_4$ tetrahedron located above the ammonium, at height $1/2$ , and a number of protons, are not shown. The off-center motion of the ammonium ion is indicated by the arrow. This is one of the four possible directions of this arrow in the (001) plane.....	9
8. Schematic representation of the antiferroelectric phase of ADP (or ADA).....	9
9. Schematic phase diagram of FE-AFE mixed glasses such as RADP. PG: proton glass, PE/FE: PE and FE phase coexistence region.....	10

## LIST OF FIGURES—CONTINUED

Figure	Page
10. Dispersion curve of $\omega(k)$ of the longitudinal mode from monatomic linear chain. At any frequency below the cutoff frequency $\omega_c = 2\sqrt{K/M}$ , two waves can propagate in both directions with opposite wave numbers.....	17
11. The determination of the Brillouin scattering angle $\theta$ .....	18
12. Symbols of scattering geometries. (a) Z(X,Y)X, (b)HV.....	19
13. Brillouin scattering set-up for small angles.....	21
14. Brillouin scattering set-up for backscattering.....	22
15. The actual experimental connection between AD/DA converter and instruments.....	23
16. A typical Brillouin spectrum. $d$ is the space between two mirrors of Fabry-Perot interferometer. FSR means free spectral range.....	24
17. Actual positions of crystal, sensor and laser beam in the closed-cycle helium refrigerator.....	25
18. (a) A set-up for pre-alignment of the Fabry-Perot interferometer mirrors. (b) The dashed line indicates the path along which the reflective mirror is moved to check the radius of interference fringes.....	29
19. A typical transmitted interference pattern of a Fabry-Perot etalon.....	30
20. (a) An illustrated Brillouin spectrum with larger $FSR = \alpha$ . R and B indicate the Rayleigh and Brillouin peaks, respectively. (b) An illustrated Brillouin spectrum with smaller $FSR = \alpha/2$ .....	31
21. The Debye, Cole-Cole and Cole-Davison relaxation distribution functions.....	40

## LIST OF FIGURES—CONTINUED

Figure	Page
22. Schematic representations of the properties of simple circuit combinations of ideal, frequency-independent elements of capacitance $C$ , conductance $G$ or resistance $R$ , and inductance $L$ , as shown in first column. The second column gives the complex impedance plot $Z$ , the third the complex admittance plot $Y$ and the fourth the complex capacitance $C^*$ . The fifth column gives the corresponding plots of $\log C'(\omega)$ (solid line) and $\log C''(\omega)$ (dotted line), against $\log \omega$ . Arrows indicate the sense of increasing frequency. Vertical and horizontal axes are imaginary and real parts, respectively.....	45
23. Light scattering diagram.....	47
24. Momentum conservation of photons and phonon.....	51
25. Index ellipsoid. Two waves, polarized along $\bar{D}_1$ and $\bar{D}_2$ (mutually orthogonal), can propagate in the $\bar{k}$ direction (applicable to both incident and scattered beams), with different velocities.....	53
26. Orientations of phonon propagation wave vector $\bar{q} // [100]$ and three wave polarizations.....	59
27. Orientations of phonon propagation wave vector $\bar{q} // [110]$ and three wave polarizations.....	61
28. Orientations of phonon propagation wave vector $\bar{q} // [\cos\theta, \sin\theta, 0]$ and three wave polarizations.....	62
29. (a) Elasticity vs. temperature for (i) $\beta\eta\mu$ linear coupling, (ii) $\gamma\eta^2\mu$ quadratic coupling, solid line for either second-order or first-order and dotted line only for first-order and (iii) $\alpha\eta\mu^2$ coupling. (b) The dynamic effects for a second-order $\eta^2\mu$ -type quadratic coupling in typical pure ferroelectrics. $\nu$ is phonon frequency shift and $\delta$ is phonon damping.....	73
30. Anti-Stokes components of the LA[100] Brillouin frequency shift for temperatures around the maximum value of half-width for DRDA. The open circles are the measured data and solid lines are the Lorentz fits.....	81

## LIST OF FIGURES—CONTINUED

Figure	Page
31. Anti-Stokes components of the LA[100] Brillouin frequency shift for temperatures around the maximum value of half-width for DRADA-0.10. The open circles are the measured data and solid lines are the Lorentz fits.....	82
32. Anti-Stokes components of the LA[100] Brillouin frequency shift for temperatures around the maximum value of half-width for DRADA-0.28. The open circles are the measured data and solid lines are the Lorentz fits.....	83
33. Frequency shift and half-width vs. temperature of the LA[100] phonons for DRDA. The solid line for frequency shift is the Debye anharmonic calculation with parameters from Table 1. The dashed line and solid circles for half-width are the qualitative estimates for the Landau-Khalatnikov and pure lattice anharmonic contributions, respectively. The error bar indicates the error range for the half-width experimental points.....	84
34. Frequency shift and half-width vs. T of the LA[100] phonons for DRADA-0.10. The solid line for frequency shift is the Debye anharmonic calculation with parameters from Table 1. The solid line and solid circles for half-width are the estimates of fluctuations and pure lattice anharmonic contributions, respectively. The dashed line is a guide to the eye. The error bar indicates the error range for the half-width experimental points.....	85
35. Frequency shift and half-width vs. temperature of the LA[100] phonons for DRADA-0.28. The solid line for frequency shift is the Debye anharmonic calculation with parameters from Table 1. The dashed line is a guide to the eye. The error bar indicates the error range for the half-width experimental points.....	86
36. The temperature dependence of the real part of the dielectric relative permittivity in NBT at two frequencies upon heating. The A, B, and C arrows indicate three anomalous regions.....	94
37. Comparison of the dielectric anomaly in region A. The curves 3 and 4 show only heating and cooling runs, respectively. The inset shows that this anomaly is hidden by an increasing background at lower frequencies.....	95
38. The temperature dependences of remanent polarization, $P_r$ , and dielectric permittivity ( $\epsilon'$ ) upon heating in region B where a ferroelectric state exists.....	96

## LIST OF FIGURES—CONTINUED

Figure	Page
39. The real part of dielectric permittivity vs. temperature in region C at various frequencies upon heating. The solid line is the calculation of Eq. (41) with $N=54$ and dashed line is the calculation of Eq. (41) with $N=125$ .....	97
40. (a) The temperature dependence of the real part ( $\epsilon'$ ) of the dielectric permittivity in NBT and PMN at 100 Hz upon cooling. (b) The temperature dependence of the imaginary part ( $\epsilon''$ ) of the dielectric permittivity in NBT and PMN at 100 Hz upon cooling.....	98
41. (a) $\sigma(=2\pi f\epsilon_0\epsilon'')$ vs. temperature at five different frequencies. The solid line is the fit of Eq. (121) for $\sigma_c$ with parameters $\sigma_0=2.12\times 10^7 (\Omega m)^{-1}$ and $w=18860$ K. (b) The imaginary part of dielectric permittivity, $\epsilon''_p=\Delta\sigma/(2\pi f\epsilon_0)$ , vs. temperature at five different frequencies. $\Delta\sigma=\sigma-\sigma_c$ .....	99
42. Complex representation of the NBT dielectric permittivity at four different temperatures. The numbers on the points indicate the frequencies in Hz. The dashed lines are regression lines.....	100
43. The strong thermal hysteresis behavior in region C at four different frequencies (10 kHz and 100 kHz in the left inset). Right inset: the difference of heating and cooling peak values shows a drop in the region of the ferroelastic phase transition at $T_{c1}\sim 820$ K. The numbers on the points indicate the frequencies in kHz. The dashed line is a regression line.....	101
44. The temperature behavior of dc permittivity, $\epsilon'$ , calculated from Eq. (41) with $N=125$ . Inset: solid hexagons are from Eq. (41) with $N=125$ , squares are the "measured" dc permittivity, solid circles are proportional to the tetragonal order parameter from neutron scattering, and triangles are the calculated dc permittivity as defined by the dc permittivity from Eq. (41) multiplied by the tetragonal order parameter. All curves are adjusted to cross at 800 K.....	102
45. Relaxation times, $\tau_{pk}$ and $\tau_{RC}$ , vs. $1000/T$ . The solid and dashed lines are fits of equation $\tau=\tau_0 e^{W/T}$ with $\tau_0=5.57\times 10^{-18}$ s, $W=25090$ K for $\tau_{pk}$ , and $\tau_0=3.54\times 10^{-21}$ s, $W=30720$ K for $\tau_{RC}$ .....	103

## LIST OF FIGURES—CONTINUED

Figure	Page
46. The real part of dielectric relative permittivity $10^{-4} \epsilon'$ vs. frequency (Hz) at five temperatures. The solid curves are fits of Eq. (34) with parameters of Table 2.....	104
47. (a) A actual connection of sample and electrods. (b) A series of two parallel RC circuits. $Z_1^{-1} = \frac{1}{R_1} + i\omega C_1$ and $Z_2^{-1} = \frac{1}{R_2} + i\omega C_2$ .....	105
48. Plots of Eq. (124) with parameters: $d_{\text{bulk}}=1$ mm, $d_{\text{sur}}=10^{-4}$ mm, $W_{\text{bulk}}=20000$ K, $W_{\text{sur}}=30000$ K, $\epsilon'_{\text{bulk}}=\epsilon'_{\text{sur}}=100$ , and $\sigma_0=10^7$ (ohm-m) $^{-1}$ .....	107
49. Brillouin backscattering spectra of NBT at different temperatures near the damping maximum.....	112
50. Damping of the longitudinal acoustic phonons vs. temperature in the vicinity of the cubic-tetragonal phase transition.....	113
51. Temperature dependence of different characteristics in NBT: (a) Brillouin shift of the longitudinal acoustic phonons vs. T. (b) Half-width of Brillouin components vs. T. (c) Intensity of the background vs. T.....	114
52. Intensity of the superlattice reflections from M and R points of the cubic Brillouin zone obtained in neutron scattering measurements vs. T to show the range of phase coexistence (shaded region). The phase sequence in NBT is shown at the top; I:paraelectric and paraelastic, II:ferroelastic, III:antiferroelectric(?), IV: ferroelectric. The corresponding crystal symmetries are shown in the middle. All data were obtained on heating runs.....	115
53. Anti-Stokes and Stokes components of the LA[001] Brillouin spectra for temperatures near the maximum damping value for $\theta_s=180^\circ$ in PMN. The frequency interval between two the Rayleigh peaks is 17.035 GHz (FSR).....	119
54. (a) Frequency shift and (b) Half-width vs. temperature of the LA[001] phonons for $\theta_s=180^\circ$ . (c) The real part of dielectric permittivity vs. temperature at four different frequencies. The dashed line indicates the ferroelectric phase transition temperature $T_c \sim 212$ K.....	120

## LIST OF FIGURES—CONTINUED

Figure	Page
55. (a) Frequency shift and (b) Half-width vs. temperature of the LA[001] phonons for $\theta_s=32.6^\circ$ . (c) Frequency shift vs. temperature of the TA[001] phonons. The dashed line is a guide to the eye.....	121
56. (a) Frequency shift and (b) Half-width vs. temperature of the LA[001] phonons for $\theta_s=12.6^\circ$ . (c) Frequency shift vs. temperature of the TA[001] phonons. The dashed line is a guide to the eye.....	122

## ABSTRACT

Temperature and frequency dependent measurements of dielectric permittivity, acoustic sound velocity and damping have been carried out by using Brillouin light scattering and a capacitance and conductance component analyzer on two different types of ferroelectrics, i.e. (i) FE-AFE mixed deuteron glasses  $\text{Rb}_{1-x}(\text{ND}_4)_x\text{D}_2\text{AsO}_4$  ( $x=0, 0.10, 0.28$ ), (ii) relaxor ferroelectrics  $\text{Na}_{1/2}\text{Bi}_{1/2}\text{TiO}_3$  (NBT) and  $\text{PbMg}_{1/3}\text{Nb}_{2/3}\text{O}_3$  (PMN).

In this study, three important results have been observed: (1) A broad and high-value maximum in dielectric permittivity has been observed in relaxors NBT and PMN, which indicates that these materials could be used for electrostrictive displacement transducers. (2) In FE-AFE mixed glasses DRADA- $x$ , a  $\eta^2\mu$ -type quadratic coupling, squared in order parameter and linear in strain, becomes the main coupling contribution as ammonium  $\text{ND}_4$  concentration  $x$  increases from 0 to an intermediate value. The results also confirm the presence of PE/FE phase coexistence in DRADA-0.10. (3) For both FE-AFE mixed glasses and relaxor ferroelectrics, the order parameter(s) fluctuations, which are generated by the local random fields originating from short-range randomly-placed cations, are the main dynamic mechanisms for hypersonic and dielectric anomalies. In DRADA-0.10 and 0.28, these local randomly-placed ions are  $\text{ND}_4^+$  and  $\text{Rb}^+$  ions. In PMN, those randomly-placed cations are  $\text{Mg}^{+2}$  and  $\text{Nb}^{+5}$  which are randomly placed at B-site positions. In NBT, those randomly-placed cations are  $\text{Na}^{+1}$  and  $\text{Bi}^{+3}$  which are placed randomly at A-site positions.

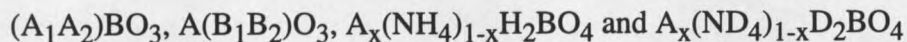
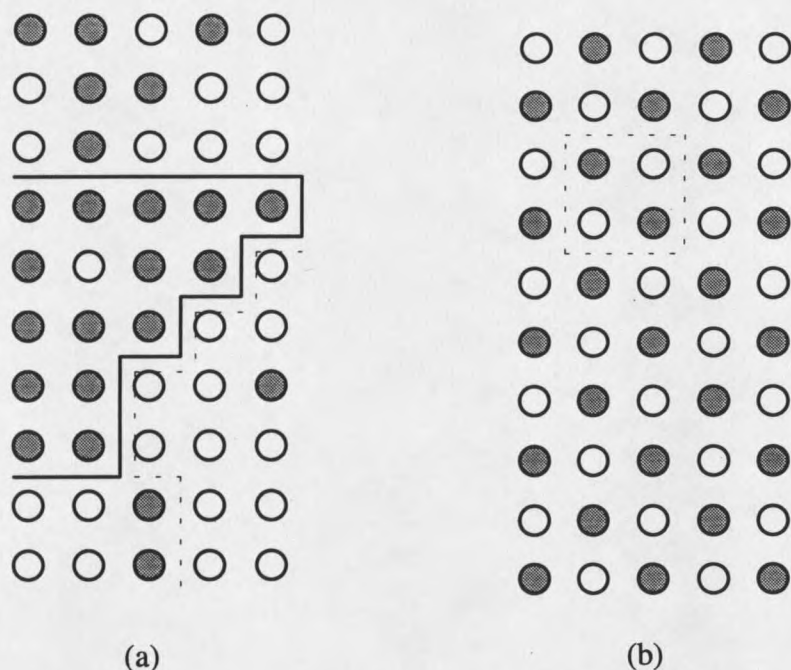
Two models, i.e. superparaelectric cluster and extrinsic bulk conductivity, also have been proposed to explain the high-temperature and low-frequency dielectric anomaly in NBT. The elastic stiffness and compliance constants are also calculated for PMN.

## CHAPTER 1

## INTRODUCTION

Introduction to Disordered Crystals

If the composition in a crystal is not completely uniform (compositional heterogeneity) down to the unit cell scale or has cation fluctuations statistically or dynamically, then the crystal is usually called "disordered".<sup>1</sup> In terms of symmetry, "disordered" means that there is no long-range translational symmetry inside the crystal. Among disordered materials, many experiments have concentrated on two different systems, i.e. ferroelectric (FE)-antiferroelectric (AFE) mixed crystals with the general formula  $A_{1-x}(NH_4)_xH_2BO_4$  [ $A=Rb, K, Cs$  and  $Tl, B=P$  and  $As$ ]<sup>2-11</sup> and complex relaxor ferroelectrics with formula  $(A'_x A''_{1-x})^{+2} B^{+4} O_3^{-2}$  or  $A^{+2} (B'_x B''_{1-x})^{+4} O_3^{-2}$ .<sup>1,12,13</sup> In these systems, local random fields originating from randomly-placed cations (or ions) play an important role for physical properties such as acoustic (sound velocity and damping) and dielectric anomalies. Since local random fields can suppress the long-range electric ordering and produce the order parameter fluctuations, a normal sharp phase transition usually is not observed in these materials. "Diffuse" (non-sharp peak) phase transition is the typical anomalous characteristic of these disordered materials. The two-dimensional distributions of ions (or cations) for both ordered and disordered states are given schematically in Fig. 1.



Disordered State

— $A_1(\bullet)$ ,  $B_1(\bullet)$  or  $A(\bullet)$  rich region

⋯ $A_2(O)$ ,  $B_2(O)$  or  $NH(D)_4(O)$  rich region

Ordered State

Uniform composition

Full translational symmetry

Figure 1. Two-dimensional illustrations of ordered and disordered states for both FE-AFE mixed glasses  $A_x(NH_4)_{1-x}H_2BO_4$  [or  $A_x(ND_4)_{1-x}D_2BO_4$ ] and complex relaxor ferroelectric systems  $(A_1A_2)BO_3$ ,  $A(B_1B_2)O_3$ .

For relaxor ferroelectrics, one can use thermal treatments such as annealing, quenching and ratio of cations to control ordering.<sup>1</sup> In FE-AFE mixed proton glasses, the crystal ordering depends on ammonium concentration.<sup>2-7</sup> From experimental results, some general differences have been found between ordered and disordered ferroelectrics:

(1) Ordered (normal):

- a) Sharp dielectric phase transition at  $T_C$
- b) Stable remanent polarization

- c) No strong dielectric frequency dependence at phase transition
  - d) Stable birefringence
  - e) No local random fields
  - f) Usually no intermediate phase between high- and low-symmetries
- (2) Disordered:
- a) Diffuse dielectric transition which doesn't correspond to any specific change of symmetry (or phase)
  - b) No stable remanent polarization
  - c) Strong frequency dependence at diffuse transition
  - d) No stable birefringence
  - e) Strong local random fields
  - f) Usually associated with a sequence of phase transitions, i.e. one (or more) intermediate phase occurred between high- and low-symmetries

In this study, five different single crystals have been measured, i.e. FE-AFE mixed deuteron glasses,  $\text{Rb}_x(\text{ND}_4)_{1-x}\text{D}_2\text{AsO}_4$  with  $x=0, 0.10$  and  $0.28$  and complex relaxor ferroelectrics,  $\text{Pb}(\text{Mg}_{1/3}\text{Nb}_{2/3})\text{O}_3$  (PMN) and  $\text{Na}_{1/2}\text{Bi}_{1/2}\text{TiO}_3$  (NBT). The introductions to these two different systems are given below.

### Relaxor Ferroelectrics (RF)

Perovskite is the name of the mineral calcium titanate ( $\text{CaTiO}_3$ ). Most of the useful piezoelectric (ferroelectric) crystals, such as barium titanate ( $\text{BaTiO}_3$ ), lead titanate ( $\text{PbTiO}_3$ ), lead zirconate titanate ( $\text{PbZr}_{1-x}\text{Ti}_x\text{O}_3$ ), lead lanthanum zirconate titanate (PLZT), sodium bismuth titanate  $\text{Na}_{1/2}\text{Bi}_{1/2}\text{TiO}_3$  and lead magnesium niobate  $\text{Pb}(\text{Mg}_{1/3}\text{Nb}_{2/3})\text{O}_3$  etc., have perovskite-type structure, i.e.  $\text{ABO}_3$ -type unit cell.<sup>13</sup> Here "O" is oxygen, "A" represents a cation with a larger ionic radius, and "B" a cation with a

smaller ionic radius. Fig. 2 shows a typical cubic  $ABO_3$  perovskite-type structure in the paraelectric phase and possible directions of distortion in the ferroelectric phase.<sup>14</sup>

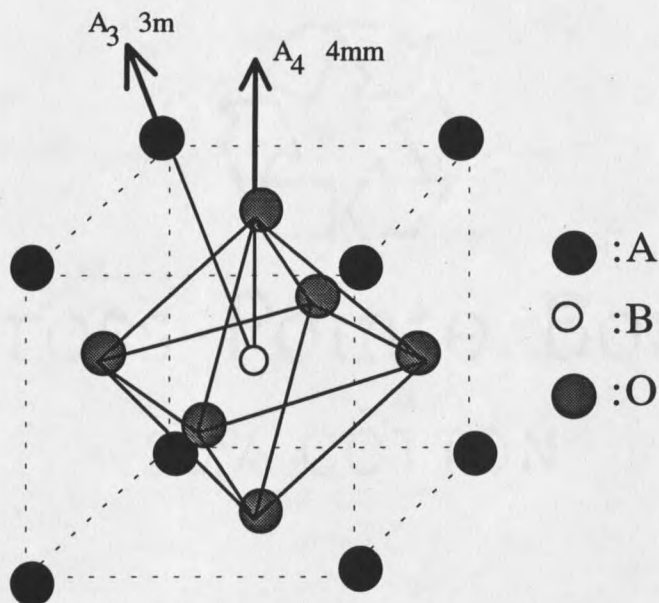


Figure 2. A perovskite cubic unit cell. The point group usually is  $m\bar{3}m$  for a paraelectric cubic  $ABO_3$  perovskite-type structure. Solid lines indicate the  $BO_6$  octahedron.  $A_4$  indicates one of three 4-fold rotation axes and  $4mm$  is the usual corresponding point group in the tetragonal ferroelectric phase.  $A_3$  indicates one of four 3-fold rotation axes and  $3m$  is the usual corresponding point group in the trigonal ferroelectric phase.

Many of the complex relaxor ferroelectrics with perovskite-type structure are compounds with either  $A^{+2}B^{+4}O_3^{-2}$  or  $A^{+1}B^{+5}O_3^{-2}$ -type formula. In the perovskite family, there are many compounds with the formula  $A^{+3}B^{+3}O_3^{-2}$ , but among them no ferroelectrics have been discovered.<sup>13</sup>

The perovskite structure is essentially a three-dimensional network of  $BO_6$  octahedra (see Fig. 2). It may also be regarded as a cubic close-packed arrangement of A and B ions with B ions filling the octahedral interstitial positions.<sup>13</sup> The packing situation of this structure may be characterized by a tolerance factor  $t$ , which is defined by the following equations:<sup>13</sup>

$$R_A + R_O = t\sqrt{2}(R_B + R_O) \quad (1)$$

or

$$t = \frac{R_A + R_O}{\sqrt{2}(R_B + R_O)} \quad (2)$$

where  $R_A$ ,  $R_B$  and  $R_O$  are the ionic radii of A, B and O ions, respectively. When  $t$  is equal to 1, the packing is said to be ideal. When  $t$  is larger than 1, there is too large a space available for the B ion, and therefore this ion can "move" inside its octahedron. In general, to form a stable perovskite structure, one requires that  $0.9 < t < 1.1$ . Besides the ionic radii, other factors, such as polarizability and character of bonds, must also be taken into account.<sup>13</sup>

The term "complex relaxor ferroelectrics" generally refers to the complex perovskites in which the charge classifications of  $(A'_x A''_{1-x})^{+2} B^{+4} O_3^{-2}$  or  $A^{+2} (B'_x B''_{1-x})^{+4} O_3^{-2}$  etc. are satisfied and unlike-valence cations belonging to a given site (A or B) are present in the correct ratio for charge balance, but are situated randomly on these cation sites. For example, sodium bismuth titanate  $Na_{1/2}Bi_{1/2}TiO_3$  has two unlike valence cations  $Na^+$  and  $Bi^{+3}$  distributed in the A site and lead magnesium niobate  $Pb(Mg_{1/3}Nb_{2/3})O_3$  has two unlike valence cations  $Mg^{+2}$  and  $Nb^{+5}$  distributed in the B site.<sup>1,15,16</sup> These randomly different cation charges give rise to random electric fields and cause random elastic distortion fields in microregions. These random fields tend to make the phase transitions "diffuse" instead of sharp as in normal ferroelectrics, and complicate the task of determining structure and state of electric order. The electric properties of relaxor ferroelectrics also depends on the cation ordering degree. The degree of ordering inside a crystal depend on several things such as method of crystal growth, cation valence, and thermal treatment (e.g. quenching and annealing). In certain compounds,





































































































































































































































































